Report

Cell Reports

The AMSH3 ESCRT-III-Associated Deubiquitinase Is Essential for Plant Immunity

Graphical Abstract

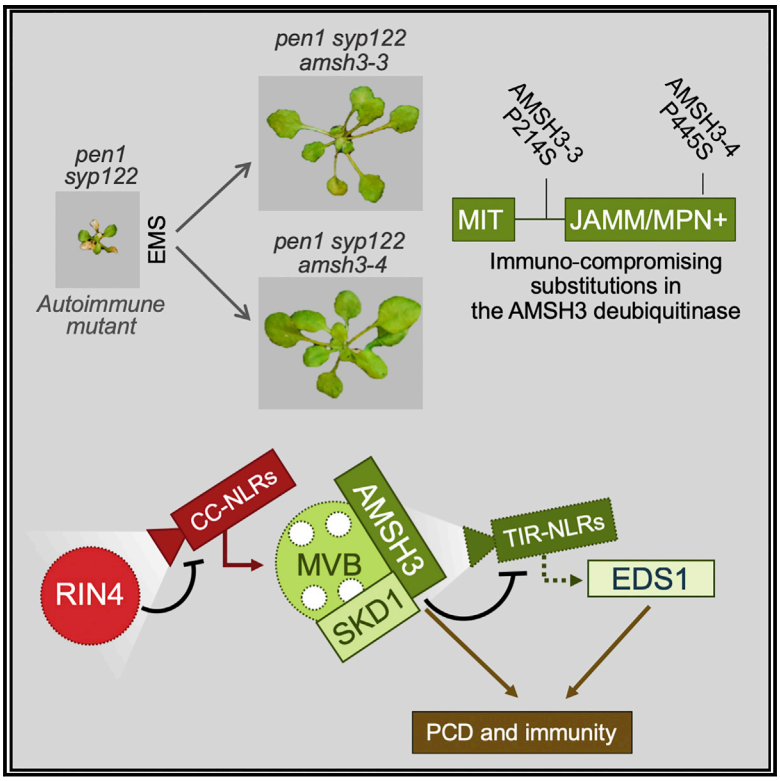

Highlights

- The ESCRT-associated deubiquitinase AMSH3 is required for autoimmunity of *pen1 syp122*
- AMSH3 activity is required for immunity mediated by the CC-NLRs, RPM1 and RPS2
- Activity of SKD1 is required for activation of PCD downstream of RPM1
- The seedling lethality of the AMSH3 knockout is EDS1 dependent

Authors

Torsten Schultz-Larsen, Andrea Lenk, Kamila Kalinowska, Lau Kræsing Vestergaard, Carsten Pedersen, Erika Isono, Hans Thordal-Christensen

Correspondence

htc@plen.ku.dk

In Brief

NLR receptors are important for plant immunity as they monitor plant processes that are targeted by pathogens. Schultz-Larsen et al. find that the AMSH3 deubiquitinase enzyme is important for immunity activated by specific NLRs. Furthermore, their results suggest that AMSH3 itself is monitored by other NLRs.

Schultz-Larsen et al., 2018, Cell Reports *25*, 2329–2338
November 27, 2018
https://doi.org/10.1016/j.celrep.2018.11.011

CellPress

Cell Reports
Report

The AMSH3 ESCRT-III-Associated Deubiquitinase Is Essential for Plant Immunity

Torsten Schultz-Larsen,[1] Andrea Lenk,[1] Kamila Kalinowska,[2,4] Lau Kræsing Vestergaard,[1] Carsten Pedersen,[1] Erika Isono,[2,3] and Hans Thordal-Christensen[1,5,*]
[1]Department of Plant and Environmental Sciences, Copenhagen Plant Science Centre, University of Copenhagen, 1871 Frederiksberg C, Denmark
[2]Department of Plant Sciences, Technical University of Munich, 85456 Freising, Germany
[3]Department of Biology, University of Konstanz, 78457 Konstanz, Germany
[4]Present address: Biochemie-Zentrum Regensburg, University of Regensburg, 93053 Regensburg, Germany
[5]Lead Contact
*Correspondence: htc@plen.ku.dk
https://doi.org/10.1016/j.celrep.2018.11.011

SUMMARY

Plant "nucleotide-binding leucine-rich repeat" receptor proteins (NLRs) detect alterations in host targets of pathogen effectors and trigger immune responses. The *Arabidopsis thaliana* mutant *pen1 syp122* displays autoimmunity, and a mutant screen identified the deubiquitinase "associated molecule with the SH3 domain of STAM3" (AMSH3) to be required for this phenotype. AMSH3 has previously been implicated in ESCRT-mediated vacuolar targeting. Pathology experiments show that AMSH3 activity is required for immunity mediated by the CC-NLRs, RPS2 and RPM1. Co-expressing the autoactive RPM1^{D505V} and the catalytically inactive ESCRT-III protein SKD1^{E232Q} in *Nicotiana benthamiana* supports the requirement of ESCRT-associated functions for this CC-NLR-activated immunity. Meanwhile, loss of ESCRT function in *A. thaliana* is lethal, and we find that AMSH3 knockout-triggered seedling lethality is "enhanced disease susceptibility 1" (EDS1) dependent. Future studies may reveal whether AMSH3 is monitored by a TIR-NLR immunity receptor.

INTRODUCTION

Plants recognize pathogen invasion using plasma membrane-bound and intracellular receptors to trigger effective immune systems (Couto and Zipfel, 2016; Jones et al., 2016). To promote disease, pathogens transfer effectors into plant cells, where they target key immunity and susceptibility components. Plants monitor intracellular effector targets using "nucleotide-binding leucine-rich repeat" receptors (NLRs) (Jones et al., 2016). When effectors modify host proteins that are monitored by NLRs, effector-triggered immunity (ETI) is activated, and a complex signaling network translates it into an immune response involving the activation of hundreds of genes and often programmed cell death (PCD) of one or more cells (Jones et al., 2016; Spoel and Dong, 2012).

ETI activation follows different genetic pathways that are dependent on specific NLR N-terminal domains. In *Arabidopsis thaliana*, ETI activated by Toll-like/interleukin-1 receptor (TIR)-NLRs (TNLs) is dependent on "enhanced disease susceptibility 1" (EDS1) and PAD4, while ETI activated by coiled-coil (CC)-NLRs (CNLs) can require "non-race specific disease resistance 1" (NDR1) (Aarts et al., 1998; Wiermer et al., 2005; Day et al., 2006). Two CNLs, RPM1 and RPS2, mediate NDR1-dependent ETI when RIN4 is phosphorylated and cleaved by the bacterial effectors AvrRpm1 and AvrRpt2, respectively. A third CNL, RPS5, mediates NDR1-dependent but RIN4-independent ETI (Jones et al., 2016). The TNL RPS4 activates EDS1-dependent ETI when RRS1-R is either acetylated by PopP2 or bound to AvrRps4 (Sarris et al., 2015). Screening for *A. thaliana* mutants with enhanced disease susceptibility has led to the identification of important immunity signaling components. Examples are EDS1, PAD4, and NDR1, which are required for NLR signaling. Meanwhile, SID2, EDS5, NPR1, and FMO1 are associated with salicylic acid (SA) and pipecolic acid (Pip) signaling, contributing to NLR activation of ETI (Wiermer et al., 2005; Zeier, 2013; Jones et al., 2016).

An alternative approach, based on lesion mimic mutants (LMMs) that exhibit constitutive autoimmune responses, has been highly successful for identifying novel immune components. Re-mutagenesis screens of LMMs have identified several defense components, such as 14 *MOS* genes (Johnson et al., 2012). Other examples are the *LAZ* genes identified in rescuing screens of *acd11* (Rodriguez et al., 2016). It has been proposed that LMM phenotypes can be caused by the activation of NLRs, when guarded proteins, possibly pathogen effector targets, are lost due to mutations (Lolle et al., 2017; Rodriguez et al., 2016). Thus, *rin4* is a severe LMM, rescued by *rps2 CNL* gene mutations (Mackey et al., 2003; Jones et al., 2016), and dependent on NDR1. Similarly, the LMM *lsd1* is rescued by mutations in *ADR1 CNL* genes (Bonardi et al., 2011; Roberts et al., 2013). Other LMMs such as *acd11*, *mpk4, smk7*, and *camta3* are partially or fully rescued by mutations in *EDS1* and by mutations in *TNL* genes (Gloggnitzer et al., 2014; Lolle et al., 2017; Rodriguez et al., 2016; Zhang et al., 2012). The fact that EDS1 and NDR1 are required for NLR-mediated ETI (Aarts et al., 1998;

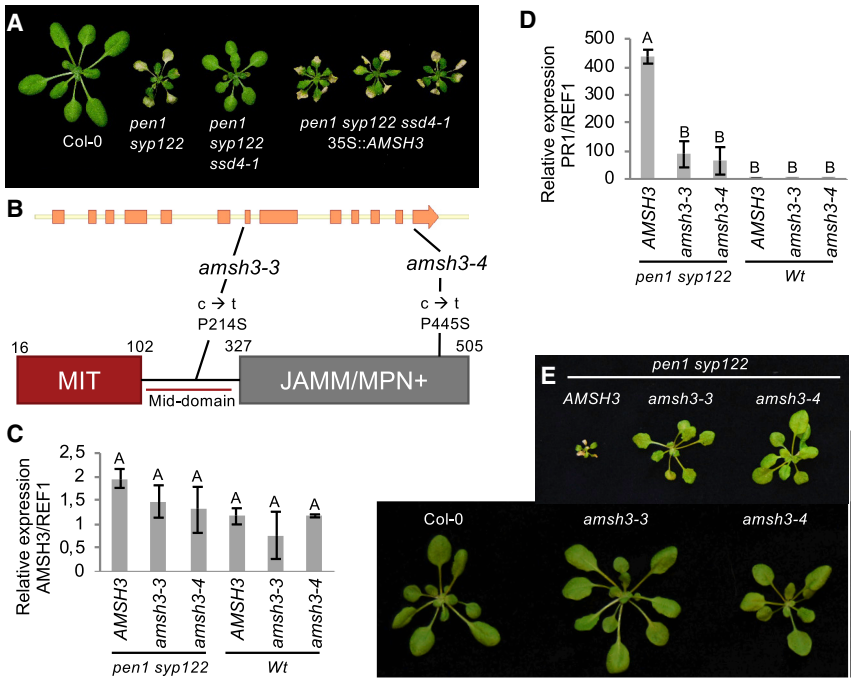

Figure 1. The Full Lesion Mimic Phenotype of *pen1 syp122* Requires *AMSH3*

(A) Representative pictures of 4-week-old plants; the *35S::AMSH3* complemented lines are independent T1 transformants.

(B) Schematic overview of the AMSH3 gene and protein.

(C and D) *AMSH3* (C) and *PR1* (D) transcript profiling performed on 4-week-old plants. Error bars, SE (n = 3). Letters denote significant differences determined by ANOVA followed by a Tukey's honestly significant difference (HSD) post hoc test.

(E) Five-week-old *pen1 syp122* rescued by the two *amsh3* mutant alleles, as well as *amsh3-3* and *amsh3-4* single mutants. These experiments have been repeated three times, with a similar result.

Wiermer et al., 2005) can therefore be used to suggest that EDS1- and NDR1-dependent LMM autoimmunity are activated by monitoring NLRs.

PEN1, also referred to as SYP121, is an *A. thaliana* plasma membrane syntaxin that is required for penetration resistance against powdery mildew fungi (Collins et al., 2003). The closest homolog of PEN1 is SYP122, and *pen1-1 syp122-1*, hereafter referred to as *pen1 syp122*, is a severe LMM that requires *EDS1*, *PAD4*, *NDR1*, *SID2*, *EDS5*, *FMO1*, *ALD1*, and *NPR1* (Zhang et al., 2007, 2008). Mutations in two of these genes can provide close-to-complete rescue of *pen1 syp122* (Zhang et al., 2008). This shows that the LMM phenotype is genuinely due to autoimmunity and not developmental deficiencies directly caused by the loss of the two syntaxins. The EDS1, PAD4, and NDR1 dependency of this autoimmunity suggests that it is mediated by both TNL(s) and CNL(s), according to the reasoning above. The identities of those NLRs are unknown.

Here, we describe *suppressor of syntaxin-related death 4* (*SSD4*), which is required for *pen1 syp122* autoimmunity. We found that *SSD4* is *AMSH3*, encoding a deubiquitinase associated with the "endosomal sorting complexes required for transport III" (ESCRT-III) machinery of multivesicular bodies (MVBs) (Isono et al., 2010), and that "associated molecule with the SH3 domain of STAM3" (AMSH3) is required for ETI activated by CNLs, RPM1, and RPS2. We present data suggesting that RPM1-mediated PCD triggered by the autoactive RPM1^{D505V} also requires SKD1, another ESCRT-III-associated component. We found that seedling lethality caused by knock out of *AMSH3* (Isono et al., 2010) is EDS1 dependent, which makes us speculate that AMSH3 may not be a vital component of the cellular machinery per se. It may instead be guarded by one or more immunity-activating TNL.

RESULTS

The Autoimmune Phenotype of *pen1 syp122* Requires AMSH3

To identify components required for *pen1 syp122* autoimmunity, an ethyl methanesulfonate (EMS) mutagenesis suppressor screen identified approximately 240 partially rescued *pen1 syp122 ssd* triple mutants (Zhang et al., 2008). Here, we describe the *pen1 syp122 ssd4-1* mutant (Figures 1A, 1E, S1, and S2). Note that the LMM phenotype of *pen syp122*, and thus the rescuing effect of *ssd4-1*, become more pronounced as the plants become older. F_1 plants of *pen1 syp122 ssd4-1* × *pen1 syp122* resembled *pen1 syp122*, and F_2 plants segregated 3:1, which is consistent with a single recessive mutation causing the partial rescue.

Map-based cloning identified *AMSH3* (At4g16144) as a candidate for *SSD4* (see STAR Methods). AMSH3 is a deubiquitinase, and the *ssd4-1* allele caused the P214S substitution (Figure 1B). qPCR showed that the *AMSH3* was upregulated 2-fold in the *pen1 syp122* mutant (Figure 1C). As transfer DNA (T-DNA) insertion alleles in *AMSH3* cause seedling lethality (Isono et al., 2010), transgene complementation was used to confirm *SSD4* being *AMSH3*. Here, *pen1 syp122 ssd4-1 p35S::AMSH3* T_1 plants were *pen1 syp122*-like (Figure 1A). Complementation analysis within our collection of partially rescued *pen1 syp122 ssd* triple mutants identified another mutation at the *AMSH3* locus, which caused the P445S substitution (Figures 1B and 1E). We designated our mutant alleles *amsh3-3* (*ssd4-1*) and *amsh3-4*, respectively, following Isono et al. (2010). Thus, the autoimmune phenotype of *pen1 syp122* requires AMSH3.

AMSH3 Function in the *pen1 syp122* Autoimmune Phenotype Is Largely Independent of SA and Pip Signaling

The autoimmune phenotype of *pen1 syp122* requires functional SA and Pip signaling (Zhang et al., 2008). To determine whether AMSH3 is required for SA and Pip signaling, we made use of the mutant alleles *sid2-1*, *eds1-2*, *eds5-3*, *fmo1-1*, *pad4-19*, and *npr1-1* (Zhang et al., 2008). We introduced these six alleles

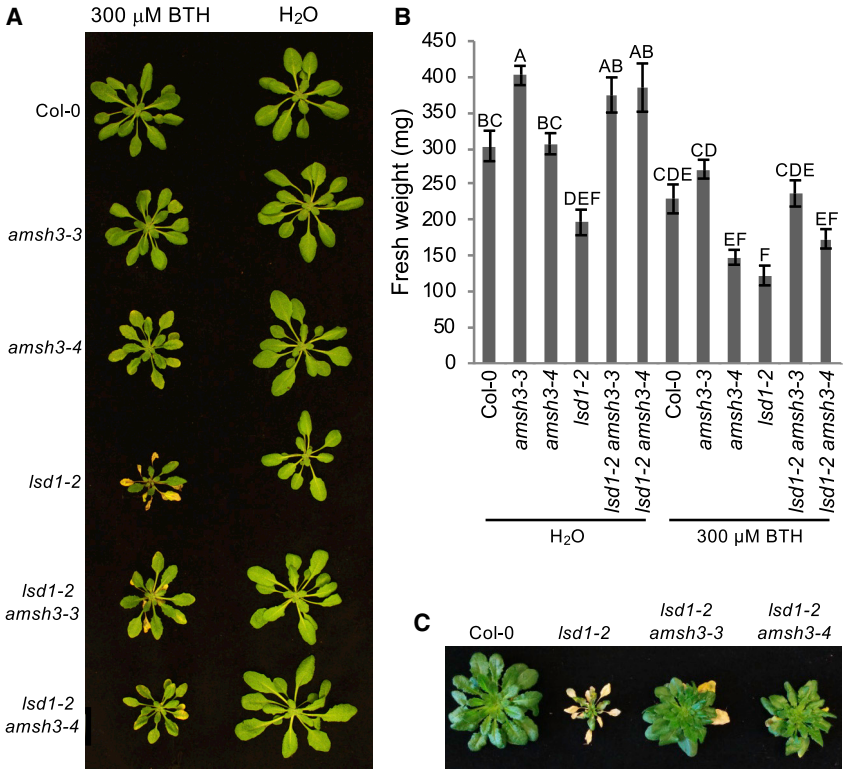

Figure 2. *AMSH3* Is Required for *lsd1*-Dependent *rcd*

(A and B) Phenotype (A) and rosette fresh weight (B) of 3-week-old plants, sprayed with 300 mM BTH or H_2O 7 days earlier. Error bars, SE (n = 9). For statistics, see Figure 1. The experiment was repeated three times, with a similar result.

(C) Thirteen-week-old short-day-grown plants, in which 3 weeks were at 20°C and then 10 weeks at 4°C. The experiments were repeated twice, with a similar result.

AMSH3 Is Required for ADR1-L1 and ADR1-L2-Dependent PCD

To obtain further insights into the biological relevance of AMSH3, the *amsh3-3* and *amsh3-4* single mutants were isolated after crossing to Col-0. They were developmentally similar to wild-type, but *amsh3-3* plants were slightly larger and *amsh3-4* plants slightly smaller than Col-0 (Figure 1E). In these 5-week-old plants, an age-related senescence phenotype appeared earlier on *amsh3-4* plants than on Col-0. *AMSH3* expression in *amsh3-3* and *amsh3-4* did not deviate from wild-type Col-0 (Figure 1C).

We found that AMSH3 was required for *pen1 syp122* autoimmunity, but it was not directly involved in SA and Pip signaling. To determine whether AMSH3 is required for cell death in other autoimmune mutants, we introduced *amsh3-3* and *amsh3-4* into the *lsd1-2* and *acd11-2* mutants (Figures 2C and S3). *lsd1-2* has runaway cell death (*rcd*) governed by the CNLs ADR1-L1 and ADR1-L2 (Bonardi et al., 2011; Roberts et al., 2013), while *acd11* has an autoimmune cell death phenotype that is dependent on the TNL LAZ5 (Rodriguez et al., 2016). The *lsd1* autoimmune reaction can be enhanced by treatment with the SA analog bentothiadiazole (BTH). Seven days after BTH treatment, *lsd1-2* plants showed typical *rcd*, whereas Col-0 wild-type *amsh3-3* and *amsh3-4* plants did not (Figure 2A). The *lsd1-2 amsh3-3* and *lsd1-2 amsh3-4* plants showed reduced *rcd* (Figures 2A and 2B), suggesting that AMSH3 is also required for the autoimmunity of *lsd1-2* (see below regarding the intermediate effect of *amsh3-4*). Low temperature treatment also triggers *rcd* in *lsd1-2* (Huang et al., 2010), which was strongly suppressed in the *lsd1-2 amsh3-3* and *lsd1-2 amsh3-4* (Figure 2C). However, introducing the *amsh3-3* or *amsh3-4* allele into *acd11* failed to rescue its autoimmunity (Figure S3).

EDS1 Is Required for *amsh3-4* Petiteness

We have noted that *amsh3-4* plants, but not *amsh3-3* plants, were significantly smaller than Col-0 wild-type after BTH application (Figures 2A and 3A). We therefore speculated that *amsh3-4* displays a weak autoimmune phenotype. For this reason, we introduced the *eds1-2* allele into *amsh3-3* and *amsh3-4* plants. The growth of *amsh3-4* was recovered by the *eds1-2* mutation, and the fresh weight of *amsh3-4 eds1-2* was

into the *pen1 syp122 amsh3-3* triple mutant by crossing with triple mutants, in which they were already combined with *pen1* and *syp122* (all of these six triple mutants were partially rescued [Zhang et al., 2008; Figures S1 and S2]). The resulting quadruple mutants (e.g., *pen1 syp122 pad4-19 amsh3-3*) were larger than their triple mutant parents, suggesting that the AMSH3 function in *pen1 syp122*-conditioned autoimmunity is independent of SID2, EDS1, EDS5, FMO1, PAD4, and NPR1 (Figure S1). The *pen1 syp122 npr1-1* triple mutant shows bleaching of the rosette, caused by SA hyperaccumulation (Zhang et al., 2007, 2008) (Figure S2A); and the *pen1 syp122 npr1-1 amsh3-3* mutant also had bleached rosettes and stems (Figures S2A and S2B). As this phenotype is absent (e.g., after introducing *sid2-1*, which prevents SA accumulation, into *pen1 syp122 npr1-1* [Zhang et al., 2008]), this suggested that SA accumulation still occurred in the presence of *amsh3-3*. Thus, the function of AMSH3 in autoimmunity did not appear to influence SA biosynthesis and signaling. This was corroborated by the fact that the expression of the NPR1-dependent SA marker gene PR1 (Cao et al., 1997) was only reduced by 80%–85% when *pen1 syp122* was partially rescued by the *amsh3-3* and *amsh3-4* mutant alleles (Figure 1D); this suggests that SA signaling was largely independent of AMSH3. FMO1 plays a central role in Pip signaling (Zeier, 2013), and *pen1 syp122 fmo1-1 amsh3-3* was also larger than the respective triple mutants (Figure S1). In summary, the genetic epistasis analysis suggests that the AMSH3 function in the *pen1 syp122* autoimmunity is largely independent of SA- and Pip-signaling sectors.

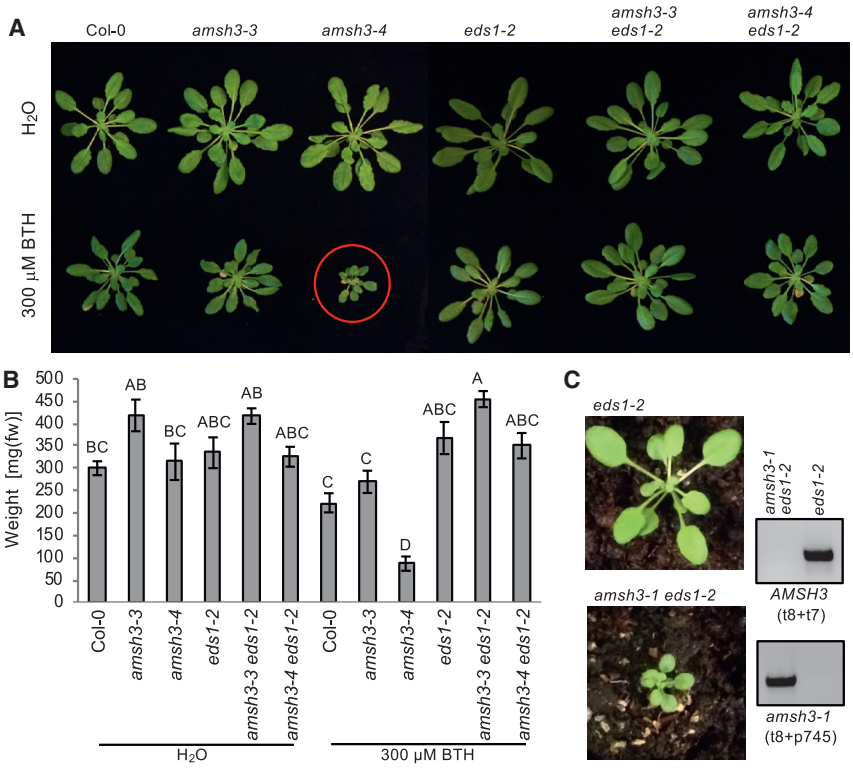

Figure 3. EDS1 Is Required for *amsh3-1* Lethality and *amsh3-4* Petiteness

(A and B) Phenotype (A) and rosette fresh weight (B) of 3-week-old plants, sprayed with 300 mM BTH or H_2O 18 days earlier. Error bars, SE (n = 6–8). For statistics, see Figure 1. The experiment was repeated three times, with a similar result.

(C) Genotyped 4-week-old individuals from a segregating population from an *amsh3-1* (+/−) *eds1-2* parent. The *AMSH3* wild-type and T-DNA insertion alleles were distinguished by PCR using *AMSH3* primers (t8 and t7) and a T-DNA primer (p745).

indistinguishable from *eds1-2* single mutants (Figures 3A and 3B). Furthermore, we noted that the *amsh3-3* plants were slightly larger than Col-0, and likewise, the *amsh3-3 eds1-2* plants were slightly larger than *eds1-2*. The *amsh3-3* effect on plant weight was independent of BTH treatment (Figures 3A and 3B). *amsh3-3* and *amsh3-4* had opposing effects on the BTH response, despite that both alleles rescued the autoimmune phenotypes of *pen1 syp122*.

The T-DNA insertion null mutations *amsh3-1* and *amsh3-2* and the ectopic overexpression of catalytically inactive AMSH3^{AXA} cause developmental arrest and seedling lethality (Isono et al., 2010). Because this could be due to the aberrant activation of defense, similar to what the phenotype of *amsh3-4 eds1-2* above suggests, we generated an *amsh3-1* (+/−) *eds1-2* (−/−) plant and analyzed the segregation of its progeny. We found that 39 plants resembled wild-type and 9 were slowly growing and dark green without necrosis (Figure 3C). This corresponds to a 3:1 segregation ratio. Genotyping confirmed that the slowly growing dark green plants were double homozygous *amsh3-1 eds1-2* mutants (Figure 3C). Thus, the seedling lethality of *AMSH3* knockout plants appears to reflect EDS1-dependent PCD.

The AMSH3 DUB Activity Appears Required for *pen1 syp122* PCD

P445, substituted in AMSH3-4, is highly conserved in JAB1/MPR1, PAD1 N-terminal+ (MPN$^+$)/Mov34 metalloenzyme (JAMM)/MPN$^+$-type deubiquitinases, and homology modeling and structure threading revealed that P445 is located in the catalytic cleft of the JAMM/MPN$^+$ DUB domain; it is sterically juxtaposed to two catalytically important histidines, Ex(n)HxH(7)S(2)D (Maytal-Kivity et al., 2002) (Figure 4A). Therefore, we analyzed whether AMSH3-4 and AMSH3-3 had altered substrate specificity or activity. We found that AMSH3-3 had catalytic activity comparable to that of wild-type AMSH3 protein (Figures 4B, 4C, and S5A). In contrast, AMSH3-4 had, as envisaged above, reduced catalytic activity and was unable to efficiently hydrolyze K48- and K63-linked ubiquitin oligomers *in vitro* (Figures 4B–4D). Yeast two-hybrid and subcellular localization revealed that neither AMSH3-3 nor AMSH3-4 interaction with the ESCRT components VPS2.1 and ALIX (Figures S4A and S4B) and localization to SKD1^{E232Q}-induced aggregates deviated from those of AMSH3 (Figure S4C). Thus, the LMM phenotype of *pen1 syp122* appears to require deubiquitinating enzyme (DUB) activity affected in AMSH3-4, as well as an unknown function affected in AMSH3-3.

T-DNA knock out of *AMSH3* or expression of AMSH3^{AXA} result in a dramatic accumulation of ubiquitin-conjugated proteins and developmental arrest (Isono et al., 2010). As AMSH3-4 had reduced catalytic activity, we examined the ubiquitination pattern in the *amsh3-3* and *amsh3-4* mutant plants. However, we found no significant alteration in the amount of ubiquitin-conjugated proteins between wild-type Col-0, *amsh3-3*, and *amsh3-4* plants (Figure 4E). This indicates that the altered catalytic activity of AMSH3-4 does not result in a dramatic global reorganization of the plant ubiquitinome. However, this can be observed during the induction of defense (Marino et al., 2012). Thus, we assayed global ubiquitin patterns in BTH-treated Col-0, *amsh3-3*, *amsh3-4*, *eds1-2*, *amsh3-3 eds1-2*, and *amsh3-4 eds1-2* plants. Here, BTH-treated *amsh3-4* plants experienced a dramatic increase in ubiquitin conjugates, which were significantly reduced, almost to wild-type levels, in *amsh3-4 eds1-2* (Figure 4F). Thus, the increased accumulation of ubiquitin conjugates appeared to occur in plants as a result of EDS1-dependent PCD stimulation, not as a direct result of the reduced deubiquitinase activity found for AMSH3-4.

Resistance Conferred by RPM1 and RPS2, but Not RPS4 and RPS5, Depends on AMSH3

We speculated above that guarding of a PEN1/SYP122-mediated process by NLRs causes the autoimmunity and PCD of

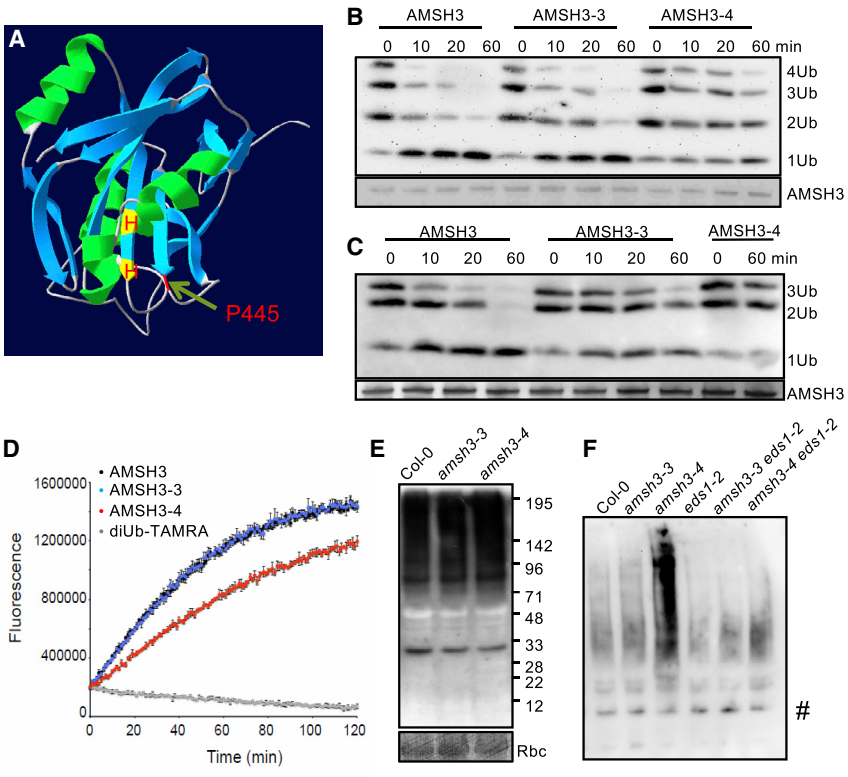

Figure 4. The P445S Substitution in AMSH3-4 Results in Reduced K48- and K63-Deubiquitinase Activity

(A) Homology model suggests that the substituted P445 in AMSH3-4 is juxtaposed to the catalytic site of the JAMM/MPN$^+$ domain. Green, α-helices. Blue, β-sheets. Yellow, catalytic H411 and H413. Red, P445 substituted in AMSH3-4.

(B and C) K48-ubiquitin tetramers (B) and K63-ubiquitin trimers (C) were incubated with AMSH3 variants *in vitro* for the indicated periods. The catalytic DUB activity was determined by the disappearance of ubiquitin oligomers visualized in the immunoblots by probing with anti-ubiquitin (top), and AMSH3, AMSH3-3, or AMSH3-4 protein levels were determined by anti-glutathione S-transferase (GST) (bottom). The experiments were repeated twice using independent AMSH3 protein purifications.

(D) *In vitro* fluorometric kinetics of AMSH3, AMSH3-3, or AMSH3-4 deubiquitinase activity using a TAMRA-based K63-linked diubiquitin. Error bars, SD (n = 4, each with three technical replicates). The experiment was repeated twice, with a similar result. See Figure S5A for gel with AMSH3 proteins.

(E) Ubiquitin conjugation in total protein extracts from 4-week-old plants visualized on an immunoblot after probing with anti-ubiquitin (top). Rubisco (Rbc) loading control (bottom). The experiment was repeated four times, with a similar result.

(F) Ubiquitin conjugation in total protein extracts from 4-week-old plants, sprayed 18 days earlier with 300 μM BTH, visualized on an immunoblot after probing with anti-ubiquitin. #, non-specific cross-reacting band serves as internal loading control.

pen1 syp122, and we have previously seen that proteins required for this autoimmunity are also required of immunity to pathogens (Zhang et al., 2007, 2008). To test whether AMSH3 is required for ETI, we spray inoculated *amsh3-3, amsh3-4*, and relevant control lines with *Pseudomonas syringae* pv. *tomato* (*Pst*) DC3000 expressing either AvrRpm1, AvrRpt2, AvrRps4, or AvrPphB. Col-0 expressed the NLRs guarding the function of these effectors (Jones et al., 2016). Increased bacterial titers of *Pst* DC3000 expressing AvrRpm1 and AvrRpt2 indicated that *amsh3-3* and *amsh3-4* were compromised in RPM1- and RPS2-conditioned resistance (Figures 5A and 5B). In contrast, bacterial titers in *amsh3-3* and *amsh3-4* mutant plants were indistinguishable from Col-0 wild-type when inoculated with *Pst* DC3000 expressing AvrPphB or AvrRps4 (Figures 5C and 5D). This suggested that *AMSH3* is required for resistance conditioned by RPM1 and RPS2, but not by RPS4 and RPS5.

RPM1- and RPS2-Dependent HR-PCD Requires AMSH3

ETI is associated with PCD at the site of infection, and consequent vacuolar rupture and cellular ion leakage can be measured as changes in media conductivity (Hofius et al., 2009). To analyze whether the AMSH3 requirement in resistance was reflected in the PCD, we challenged Col-0, *amsh3-3*, *amsh3-4*, and *ndr1-1* with *Pst* DC3000 (AvrRpm1) and tested for ion leakage. In Col-0, an increase in conductivity was observed by 3 hr post-inoculation (hpi). This increase was delayed in *amsh3-3*, *amsh3-4*, and *ndr1-1* (Figure 5E). To corroborate these findings, we performed this experiment using *Pst* DC3000 (AvrRpt2) as well. The experiment revealed that Col-0 and *amsh3-3* plants had similar conductivity kinetics, with a marked increase at ~5 hpi (Figure 5F). However, the ion leakage was considerably reduced in *amsh3-4* plants, although not to the extent seen in the *ndr1-1* control plants (Figure 5F). These results suggest that normal activation of PCD by RPM1 and RPS2 depends on AMSH3 and its catalytic deubiquitinase activity.

The *Pseudomonas* effectors AvrRpm1 and AvrRpt2 both target RIN4 to promote virulence. The CNLs RPM1 and RPS2 trigger PCD when RIN4 is altered: RPM1 is triggered by RIN4 phosphorylation and RPS2 is triggered by the loss of RIN4 interaction (Jones et al., 2016). However, overexpression of RIN4 has been shown to inhibit RPS2-dependent, although not RPM1-dependent, hypersensitive response (HR) (Mackey et al., 2003). Therefore, to test whether the effect of our *amsh3* mutations on resistance involved changes in the amount of RIN4, we made an immunoblot of the RIN4 protein. However, no difference between Col-0 wild-type, *amsh3-3*, and *amsh3-4* was found (Figure S5B). Thus, the reduced resistance to *Pst* DC3000 expressing AvrRpm1 or AvrRpt2 is not likely due to an increased steady-state level of RIN4.

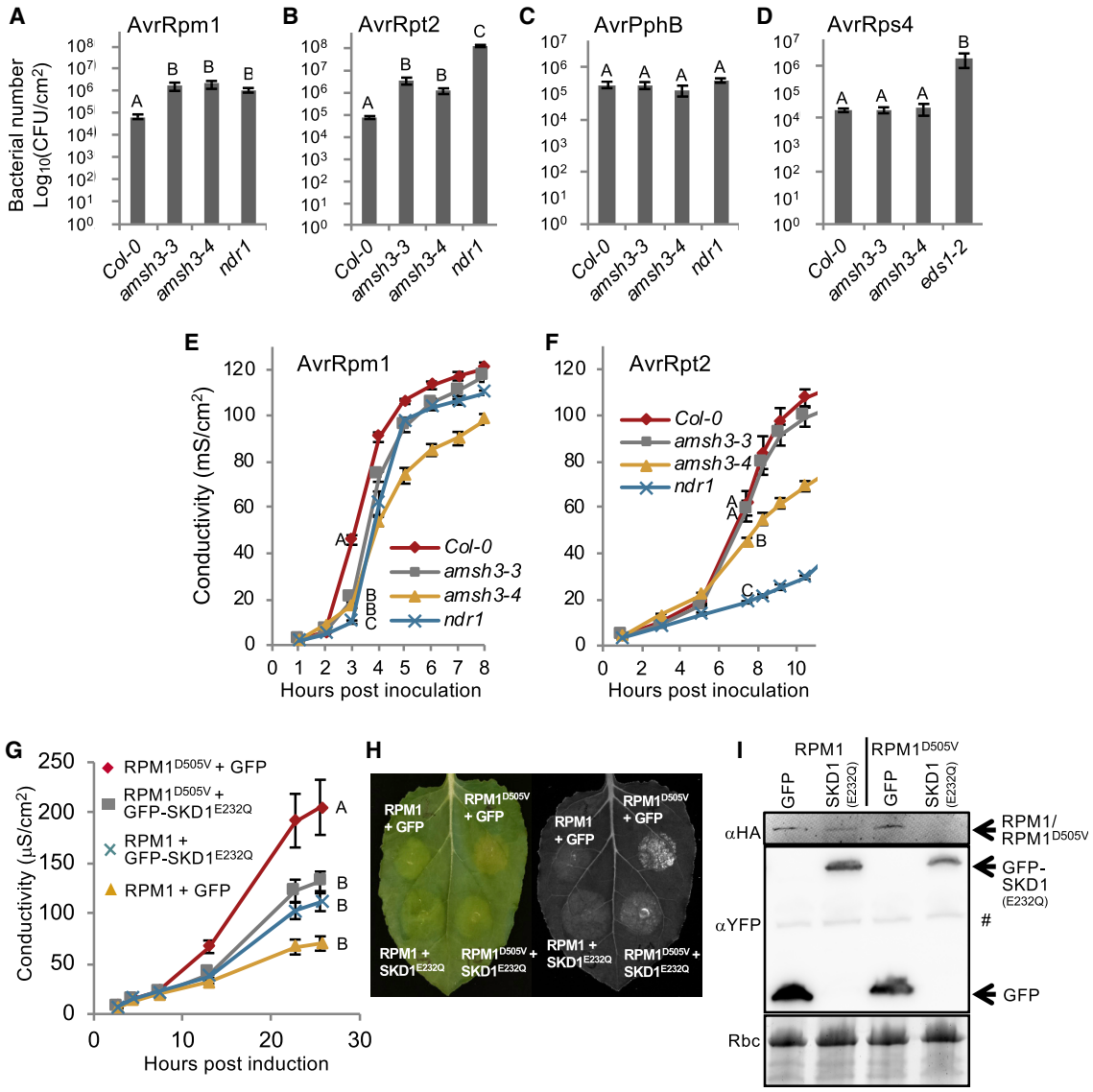

Figure 5. Involvement of AMSH3 and SKD1 in CNL-Mediated Immunity and Cell Death

(A–D) Four- to 5-week-old *A. thaliana* Col-0 plants were spray inoculated with *Pst* DC3000 expressing four different effectors: (A) AvrRpm1, (B) AvrRpt2, (C) AvrPphB, and (D) AvrRps4. The bacterial populations in the plants were determined 3 days post-inoculation (dpi). Error bars, SE (n = 12).

(E and F) For ion leakage analyses, 4-week-old *A. thaliana* Col-0 leaves were infiltrated with *Pst* DC3000 AvrRpm1 (E) and *Pst* DC3000 AvrRpt2 (F). Error bars, SE (n = 5).

(G–I) Ion leakage and HR on *N. benthamiana* leaves 2 days after *Agrobacterium*-mediated transient co-expression of the indicated proteins.

(G) GFP-SKD1^{E232Q} and GFP were 35S promoter regulated, while the expression of RPM1^{D505V} or RPM1 was induced by β-estradiol. Error bars, SE (n = 4).

(H) Leaf 3 days post-β-estradiol treatment. Left, visible light. Right, UV *trans*-illuminated.

(I) Immunoblot of total protein 5 hr after β-estradiol treatment. #, non-specific cross-reacting band. Rubisco (Rbc) loading control (bottom).

Letters denote significant differences at the indicated time points determined by ANOVA followed by a Tukey's HSD post hoc test. The experiments were repeated three times with a similar result.

Normal ESCRT-III Function Is Required for Activation of PCD Downstream of RPM1

As the AMSH3 deubiquitinase activity appeared important for immunity-related PCD, we wanted to test whether this could be due to a requirement for an intact ESCRT system. As discussed above, overexpression of SKD1^{E232Q} interferes with normal ESCRT function and stimulates MVBs to aggregate (Haas et al., 2007). Therefore, we used SKD1^{E232Q} to block ESCRT function and test for RPM1-triggered PCD. To this end, we used the autoactive RPM1^{D505V} that mimics normal RPM1 activation both in *A. thaliana* and *Nicotiana benthamiana* in the absence of RIN4^{T166} phosphorylation (Gao et al., 2011). We transiently transformed *N. benthamiana* to co-express GFP-SKD1^{E232Q} or GFP with RPM1 or RPM1^{D505V}. RPM1

co-expressed with GFP-SKD1^{E232Q} displayed elevated levels of ion leakage relative to co-expression with GFP (Figure 5G). This was consistent with a previous report showing that SKD1^{E232Q} caused cell death (Haas et al., 2007). Expression of RPM1^{D505V} triggered a rapid increase in ion leakage, which was suppressed by co-expression with GFP-SKD1^{E232Q}, despite its own activation of PCD. The level of lesion formation in *N. benthamiana* after 3 days was consistent with the conductivity assays (Figure 5H), which suggest that cell death triggered by RPM1^{D505V} requires SKD1.

The stability of GFP and GFP-SKD1^{E232Q} was apparently not affected by the co-expression with RPM1 or RPM1^{D505V} (Figure 5I). However, SKD1^{E232Q} influenced RPM1 stability. Here, the autoactive RPM1^{D505V} was not detectable when co-expressed with SKD1^{E232Q} (Figure 5I). This may suggest that activated signaling-competent RPM1 is stabilized by SKD1.

DISCUSSION

The DUB Activity of AMSH3, Conserved in Eukaryotes, Is Required for PCD

To date, the ESCRT-I components VPS28-1 and VPS37-1, as well as the SKD1/VPS4-associated protein LIP5, have been identified as positive regulators of pathogen-associated molecular pattern (PAMP)-triggered immunity (Spallek et al., 2013; Wang et al., 2014). Here, we identified the ESCRT-III-associated deubiquitinase AMSH3 as a regulator of *pen1 syp122* autoimmunity. In addition, our *amsh3* mutations were able to suppress *rcd* conditioned by *ADR1-L1* and *ADR1-L2*, as well as RPS2- and RPM1-conditioned defense responses seen as higher bacterial growth and reduced PCD. These data suggest that AMSH3 is required for PCD mediated by RPM1, RPS2, and ADR1s, all of which are CNLs. While RPM1 and RPS2 are interactors of RIN4, PCD triggered by the CNL RPS5, which is not an interactor of RIN4, did not require AMSH3. The same was true for PCD triggered by the TNL RPS4.

There are approximately 50 deubiquitinases in *A. thaliana*, and AMSH3 is 1 of 8 *A. thaliana* members of the JAMM subfamily found broadly in eukaryotes (Isono and Nagel, 2014). They are zinc metalloproteases that coordinate two zinc ions in their MPN$^+$ domain, which activates a water molecule to hydrolyze ubiquitin isopeptide bonds to lysines on target proteins. AMSH3 can hydrolyze both K48- and K63-linked ubiquitin chains (Isono et al., 2010), and the P445S substitution in the MPN$^+$ domain reduced this catalytic activity, whereas the P215S substitution did not. Proline is conformationally rigid, and it strongly affects the secondary structure of the amino acid chain in its vicinity. Therefore, a model could be that P445S affects the catalytically active site, whereas P215S affects another AMSH3 feature, which we have not been able to unravel. In summary, our observations point toward AMSH3 catalytic activity being required for autoimmunity and PCD being mediated by a subset of CNLs.

We found that AMSH3 was required for PCD triggered by AvrRpm1 and AvrRpt2 and mediated by the CNLs RPM1 and RPS2, which guard the status of RIN4. AMSH3 being an ESCRT-III component hinted that ESCRT-III in general is required for such PCD. To address this, we activated PCD in *N. benthamiana* by expressing the autoactive RPM1^{D505V} (Gao et al., 2011) and co-expressed a dominant-negative version (SKD1^{E232Q}) of the AAA-ATPase, which is essential for ESCRT-III (Haas et al., 2007). This experiment supported the AMSH3 results and suggested a general function of this pathway in PCD triggered by RPM1. These data also imply that ESCRT-III functions downstream of RIN4. Furthermore, our data suggest that the stability of the PCD signaling active but not inactive RPM1 may be influenced by the SKD1^{E232Q} mutation. This result may explain why SKD1 inactivation resulted in reduced RPM1-dependent PCD. This line of reasoning also suggests a simple model explaining why AMSH3 is required for *pen1 syp122*-dependent PCD: loss of *pen1 syp122* function triggers PCD through an NLR, the stability of which is dependent on AMSH3.

Loss of AMSH3 Triggers PCD Dependent on EDS1

AMSH3 and its closest paralog, AMSH1, share domain organization in which both have an N-terminal microtubule interacting and transport (MIT) domain, a middle domain, and a C-terminal JAMM/MPN$^+$ domain (Isono et al., 2010). *AMSH3* makes a larger contribution to development, which is evident by the fact that *amsh3-1* null mutant is seedling lethal, while the *amsh1-1* knockdown mutant displays early senescence (Isono et al., 2010; Katsiarimpa et al., 2013). Because expression of AMSH3^{AXA} also results in seedling lethality, it is the loss of AMSH3 catalytic deubiquitinase activity and not the absence of the protein that triggers PCD (Isono et al., 2010). This is consistent with the observations above, as AMSH3-4 has reduced catalytic activity and *amsh3-4* plants have reduced weight and rosette size, stimulated by BTH. It is noteworthy that both the *amsh3-1* seedling lethality and the *amsh3-4* size reduction require *EDS1*. Therefore, we suggest that these phenotypes reflect PCD governed by a TNL, as they are normally dependent on EDS1. The *amsh1* knockdown mutant displays spontaneous PCD upon pathogen challenge (Katsiarimpa et al., 2013), which is consistent with the hypothesis that an NLR response is activated.

We speculate that a TNL is triggered by the state or reduced turnover of one or more AMSH1/AMSH3-DUB substrates. This putative substrate is presumably sorted through the ESCRT system, as mutations of core ESCRT-III components (e.g., SUCROSE NONFERMENTING 7.1 [SNF7.1], VPS2.1, VPS20.1, and VPS24.1, which are affected in vacuolar trafficking) also cause seedling lethality (Katsiarimpa et al., 2013; Cai et al., 2014). Likewise, overexpression of the catalytically inactive *A. thaliana* SKD1^{E232Q} and rice SKD1^{E315Q} caused lethality in tobacco BY-2 cells and rice leaves, respectively (Haas et al., 2007; Zhu et al., 2016). Similarly, knock down of *positive regulator of SKD1* (*PROS*) or knock out of LIP5, both of which activate SKD1, has a negative effect on plant growth (Reyes et al., 2014). LIP5 interacts with ISTL1, whose yeast homolog regulates SKD1 activity (Tan et al., 2015), and the *istl1 lip5* double mutant resembles an LMM by having stunted and necrotic leaves with constitutive PR1 expression (Buono et al., 2016). These findings agree with a model in which reduced turnover of an ESCRT-III cargo activates a TNL to trigger PCD. In addition, mutations in the ESCRT-II component gene *VPS36* resemble an *amsh3-1* null mutant (Wang et al., 2017). Similarly, the ESCRT-I double mutants *vps28-1 vps28-2* and *vps37-1 vps37-2* are unable to germinate (Chikkaputtaiah, 2008).

Future studies may reveal whether these ESCRT proteins are essential, although their inhibition causes severe alterations in MVBs. They may alternatively be monitored by one or more immunity-activating NLRs. Such a model is supported by evidence put forward by Sutipatanasomboon et al. (2017), who observed *eds1*-mediated rescue of the autoimmune phenotype of the ESCRT-I component mutant *cfs1*. Thus, it is intriguing that the ESCRT pathway is dispensable in yeast (Hurley, 2015). Having observed that AMSH3 and SKD1 play positive roles in immunity, it may be biologically meaningful that NLRs guard the ESCRT-III pathway in plants.

In summary, our analyses lead us to suggest a model for a role of the ESCRT-III-associated AMSH3 and SKD1 in the execution of CNL-triggered PCD in plant immunity, and a likely guarding of these components by TNLs.

STAR★METHODS

Detailed methods are provided in the online version of this paper and include the following:

- KEY RESOURCES TABLE
- CONTACT FOR REAGENT AND RESOURCE SHARING
- EXPERIMENTAL MODEL AND SUBJECT DETAILS
  - Arabidopsis
  - Nicotiana benthamiana
  - Bacterial strains
- METHOD DETAILS
  - Map-based cloning
  - BTH-treatment
  - Plasmid constructs
  - Stable transformation of *A. thaliana* and transient protein expression in *N. benthamiana*
  - Bacterial growth assays
  - Ion leakage experiments
  - Yeast two-hybrid assay
  - Total protein extraction
  - RNA isolation and quantitative PCR
  - DUB assays
  - Protein localization in *N. benthamiana*
  - Structural homology modeling
- QUANTIFICATION AND STATISTICAL ANALYSIS

SUPPLEMENTAL INFORMATION

Supplemental Information includes five figures and one table and can be found with this article online at https://doi.org/10.1016/j.celrep.2018.11.011.

ACKNOWLEDGMENTS

We would like to thank Mette Sylvan for excellent technical assistance and Prof. Jeffery L. Dangl (University of North Carolina, USA) for sharing the pEst-T7-RPM1-YFP-HA and pEst-T7-RPM1(D505V)-YFP-HA constructs. This work was funded by the Villum Foundation, Denmark (VKR023502), and the German Science Foundation (DFG) (IS221/4-1).

AUTHOR CONTRIBUTIONS

Conceptualization, T.S.-L., A.L., and H.T.-C.; Methodology, T.S.-L., E.I., and H.T.-C.; Investigation, T.S.-L., A.L., K.K., L.K.V., and C.P.; Resources, E.I. and H.T.-C.; Writing – Original Draft, T.S.-L. and H.T.-C.; Writing – Review & Editing, T.S.-L., E.I., and H.T.-C.; Visualization, T.S.-L., E.I., and A.L.; Supervision, E.I. and H.T.-C.; Project Administration, H.T.-C.; Funding Acquisition, H.T.-C.

DECLARATION OF INTERESTS

The authors declare no competing interests.

Received: December 30, 2017
Revised: March 4, 2018
Accepted: October 31, 2018
Published: November 27, 2018

REFERENCES

Aarts, N., Metz, M., Holub, E., Staskawicz, B.J., Daniels, M.J., and Parker, J.E. (1998). Different requirements for EDS1 and NDR1 by disease resistance genes define at least two R gene-mediated signaling pathways in *Arabidopsis*. Proc. Natl. Acad. Sci. USA *95*, 10306–10311.

Bartsch, M., Gobbato, E., Bednarek, P., Debey, S., Schultze, J.L., Bautor, J., and Parker, J.E. (2006). Salicylic acid-independent ENHANCED DISEASE SUSCEPTIBILITY1 signaling in Arabidopsis immunity and cell death is regulated by the monooxygenase FMO1 and the Nudix hydrolase NUDT7. Plant Cell *18*, 1038–1051.

Biasini, M., Bienert, S., Waterhouse, A., Arnold, K., Studer, G., Schmidt, T., Kiefer, F., Gallo Cassarino, T., Bertoni, M., Bordoli, L., and Schwede, T. (2014). SWISS-MODEL: modelling protein tertiary and quaternary structure using evolutionary information. Nucleic Acids Res. *42*, W252–W258.

Bonardi, V., Tang, S., Stallmann, A., Roberts, M., Cherkis, K., and Dangl, J.L. (2011). Expanded functions for a family of plant intracellular immune receptors beyond specific recognition of pathogen effectors. Proc. Natl. Acad. Sci. USA *108*, 16463–16468.

Brodersen, P., Malinovsky, F.G., Hématy, K., Newman, M.-A., and Mundy, J. (2005). The role of salicylic acid in the induction of cell death in *Arabidopsis acd11*. Plant Physiol. *138*, 1037–1045.

Buono, R.A., Paez-Valencia, J., Miller, N.D., Goodman, K., Spitzer, C., Spalding, E.P., and Otegui, M.S. (2016). Role of SKD1 regulators LIP5 and IST1-LIKE1 in endosomal sorting and plant development. Plant Physiol. *171*, 251–264.

Cai, Y., Zhuang, X., Gao, C., Wang, X., and Jiang, L. (2014). The *Arabidopsis* endosomal sorting complex required for transport III regulates internal vesicle formation of the prevacuolar compartment and is required for plant development. Plant Physiol. *165*, 1328–1343.

Cao, H., Glazebrook, J., Clarke, J.D., Volko, S., and Dong, X. (1997). The *Arabidopsis* NPR1 gene that controls systemic acquired resistance encodes a novel protein containing ankyrin repeats. Cell *88*, 57–63.

Century, K.S., Shapiro, A.D., Repetti, P.P., Dahlbeck, D., Holub, E., and Staskawicz, B.J. (1997). NDR1, a pathogen-induced component required for *Arabidopsis* disease resistance. Science *278*, 1963–1965.

Chikkaputtaiah, C.K. (2008). Molecular and functional characterization of the Arabidopsis ESCRT-I complex. PhD dissertation (University of Cologne).

Clough, S.J., and Bent, A.F. (1998). Floral dip: a simplified method for *Agrobacterium*-mediated transformation of *Arabidopsis thaliana*. Plant J. *16*, 735–743.

Collins, N.C., Thordal-Christensen, H., Lipka, V., Bau, S., Kombrink, E., Qiu, J.L., Hückelhoven, R., Stein, M., Freialdenhoven, A., Somerville, S.C., and Schulze-Lefert, P. (2003). SNARE-protein-mediated disease resistance at the plant cell wall. Nature *425*, 973–977.

Couto, D., and Zipfel, C. (2016). Regulation of pattern recognition receptor signalling in plants. Nat. Rev. Immunol. *16*, 537–552.

Czechowski, T., Stitt, M., Altmann, T., Udvardi, M.K., and Scheible, W.R. (2005). Genome-wide identification and testing of superior reference genes for transcript normalization in *Arabidopsis*. Plant Physiol. *139*, 5–17.

Day, B., Dahlbeck, D., and Staskawicz, B.J. (2006). NDR1 interaction with RIN4 mediates the differential activation of multiple disease resistance pathways in *Arabidopsis*. Plant Cell *18*, 2782–2791.

Gao, Z., Chung, E.H., Eitas, T.K., and Dangl, J.L. (2011). Plant intracellular innate immune receptor resistance to *Pseudomonas syringae* pv. *maculicola* 1 (RPM1) is activated at, and functions on, the plasma membrane. Proc. Natl. Acad. Sci. USA *108*, 7619–7624.

Gloggnitzer, J., Akimcheva, S., Srinivasan, A., Kusenda, B., Riehs, N., Stampfl, H., Bautor, J., Dekrout, B., Jonak, C., Jiménez-Gómez, J.M., et al. (2014). Nonsense-mediated mRNA decay modulates immune receptor levels to regulate plant antibacterial defense. Cell Host Microbe *16*, 376–390.

Grant, M.R., Godiard, L., Straube, E., Ashfield, T., Lewald, J., Sattler, A., Innes, R.W., and Dangl, J.L. (1995). Structure of the *Arabidopsis* RPM1 gene enabling dual specificity disease resistance. Science *269*, 843–846.

Haas, T.J., Sliwinski, M.K., Martínez, D.E., Preuss, M., Ebine, K., Ueda, T., Nielsen, E., Odorizzi, G., and Otegui, M.S. (2007). The *Arabidopsis* AAA ATPase SKD1 is involved in multivesicular endosome function and interacts with its positive regulator LYST-INTERACTING PROTEIN5. Plant Cell *19*, 1295–1312.

Hinsch, M., and Staskawicz, B. (1996). Identification of a new *Arabidopsis* disease resistance locus, RPs4, and cloning of the corresponding avirulence gene, *avrRps4*, from *Pseudomonas syringae* pv. *pisi*. Mol. Plant Microbe Interact. *9*, 55–61.

Hofius, D., Schultz-Larsen, T., Joensen, J., Tsitsigiannis, D.I., Petersen, N.H., Mattsson, O., Jørgensen, L.B., Jones, J.D., Mundy, J., and Petersen, M. (2009). Autophagic components contribute to hypersensitive cell death in *Arabidopsis*. Cell *137*, 773–783.

Huang, X., Li, Y., Zhang, X., Zuo, J., and Yang, S. (2010). The *Arabidopsis LSD1* gene plays an important role in the regulation of low temperature-dependent cell death. New Phytol. *187*, 301–312.

Hurley, J.H. (2015). ESCRTs are everywhere. EMBO J. *34*, 2398–2407.

Isono, E., and Nagel, M.K. (2014). Deubiquitylating enzymes and their emerging role in plant biology. Front. Plant Sci. *5*, 56.

Isono, E., Katsiarimpa, A., Müller, I.K., Anzenberger, F., Stierhof, Y.D., Geldner, N., Chory, J., and Schwechheimer, C. (2010). The deubiquitinating enzyme AMSH3 is required for intracellular trafficking and vacuole biogenesis in *Arabidopsis thaliana*. Plant Cell *22*, 1826–1837.

Johnson, K.C.M., Dong, O.X., Huang, Y., and Li, X. (2012). A rolling stone gathers no moss, but resistant plants must gather their moses. Cold Spring Harb. Symp. Quant. Biol. *77*, 259–268.

Jones, J.D.G., Vance, R.E., and Dangl, J.L. (2016). Intracellular innate immune surveillance devices in plants and animals. Science *354*, aaf6395.

Kalinowska, K., Nagel, M.K., Goodman, K., Cuyas, L., Anzenberger, F., Alkofer, A., Paz-Ares, J., Braun, P., Rubio, V., Otegui, M.S., and Isono, E. (2015). *Arabidopsis* ALIX is required for the endosomal localization of the deubiquitinating enzyme AMSH3. Proc. Natl. Acad. Sci. USA *112*, E5543–E5551.

Karimi, M., Depicker, A., and Hilson, P. (2007). Recombinational cloning with plant gateway vectors. Plant Physiol. *145*, 1144–1154.

Katsiarimpa, A., Anzenberger, F., Schlager, N., Neubert, S., Hauser, M.T., Schwechheimer, C., and Isono, E. (2011). The *Arabidopsis* deubiquitinating enzyme AMSH3 interacts with ESCRT-III subunits and regulates their localization. Plant Cell *23*, 3026–3040.

Katsiarimpa, A., Kalinowska, K., Anzenberger, F., Weis, C., Ostertag, M., Tsutsumi, C., Schwechheimer, C., Brunner, F., Hückelhoven, R., and Isono, E. (2013). The deubiquitinating enzyme AMSH1 and the ESCRT-III subunit VPS2.1 are required for autophagic degradation in *Arabidopsis*. Plant Cell *25*, 2236–2252.

Koncz, C., and Schell, J. (1986). The promoter of TL-DNA gene 5 controls the tissue-specific expression of chimaeric genes carried by a novel type of *Agrobacterium* binary vector. Mol. Gen. Genet. *204*, 383–396.

Kunkel, B.N., Bent, A.F., Dahlbeck, D., Innes, R.W., and Staskawicz, B.J. (1993). *RPS2*, an *Arabidopsis* disease resistance locus specifying recognition of *Pseudomonas syringae* strains expressing the avirulence gene *avrRpt2*. Plant Cell *5*, 865–875.

Lolle, S., Greeff, C., Petersen, K., Roux, M., Jensen, M.K., Bressendorff, S., Rodriguez, E., Sømark, K., Mundy, J., and Petersen, M. (2017). Matching NLR immune receptors to autoimmunity in *camta3* mutants using antimorphic NLR alleles. Cell Host Microbe *21*, 518–529.e4.

Mackey, D., Belkhadir, Y., Alonso, J.M., Ecker, J.R., and Dangl, J.L. (2003). *Arabidopsis* RIN4 is a target of the type III virulence effector AvrRpt2 and modulates RPS2-mediated resistance. Cell *112*, 379–389.

Marino, D., Peeters, N., and Rivas, S. (2012). Ubiquitination during plant immune signaling. Plant Physiol. *160*, 15–27.

Maytal-Kivity, V., Reis, N., Hofmann, K., and Glickman, M.H. (2002). MPN+, a putative catalytic motif found in a subset of MPN domain proteins from eukaryotes and prokaryotes, is critical for Rpn11 function. BMC Biochem. *3*, 28.

Reyes, F.C., Buono, R.A., Roschzttardtz, H., Di Rubbo, S., Yeun, L.H., Russinova, E., and Otegui, M.S. (2014). A novel endosomal sorting complex required for transport (ESCRT) component in *Arabidopsis thaliana* controls cell expansion and development. J. Biol. Chem. *289*, 4980–4988.

Roberts, M., Tang, S., Stallmann, A., Dangl, J.L., and Bonardi, V. (2013). Genetic requirements for signaling from an autoactive plant NB-LRR intracellular innate immune receptor. PLoS Genet. *9*, e1003465.

Robertson, M. (2004). Two transcription factors are negative regulators of gibberellin response in the HvSPY-signaling pathway in barley aleurone. Plant Physiol. *136*, 2747–2761.

Rodriguez, E., El Ghoul, H., Mundy, J., and Petersen, M. (2016). Making sense of plant autoimmunity and 'negative regulators'. FEBS J. *283*, 1385–1391.

Sarris, P.F., Duxbury, Z., Huh, S.U., Ma, Y., Segonzac, C., Sklenar, J., Derbyshire, P., Cevik, V., Rallapalli, G., Saucet, S.B., et al. (2015). A plant immune receptor detects pathogen effectors that target WRKY transcription factors. Cell *161*, 1089–1100.

Simonich, M.T., and Innes, R.W. (1995). A disease resistance gene in *Arabidopsis* with specificity for the *avrPph3* gene of *Pseudomonas syringae* pv. *phaseolicola*. Mol. Plant Microbe Interact. *8*, 637–640.

Spallek, T., Beck, M., Ben Khaled, S., Salomon, S., Bourdais, G., Schellmann, S., and Robatzek, S. (2013). ESCRT-I mediates FLS2 endosomal sorting and plant immunity. PLoS Genet. *9*, e1004035.

Spoel, S.H., and Dong, X. (2012). How do plants achieve immunity? Defence without specialized immune cells. Nat. Rev. Immunol. *12*, 89–100.

Sutipatanasomboon, A., Herberth, S., Alwood, E.G., Häweker, H., Müller, B., Shahriari, M., Zienert, A.Y., Marin, B., Robatzek, S., Praefcke, G.J.K., et al. (2017). Disruption of the plant-specific *CFS1* gene impairs autophagosome turnover and triggers EDS1-dependent cell death. Sci. Rep. *7*, 8677.

Tan, J., Davies, B.A., Payne, J.A., Benson, L.M., and Katzmann, D.J. (2015). Conformational changes in the endosomal sorting complex required for the transport III subunit Ist1 lead to distinct modes of ATPase Vps4 regulation. J. Biol. Chem. *290*, 30053–30065.

Torres, M.A., Jones, J.D., and Dangl, J.L. (2005). Pathogen-induced, NADPH oxidase-derived reactive oxygen intermediates suppress spread of cell death in *Arabidopsis thaliana*. Nat. Genet. *37*, 1130–1134.

Wang, F., Shang, Y., Fan, B., Yu, J.Q., and Chen, Z. (2014). *Arabidopsis* LIP5, a positive regulator of multivesicular body biogenesis, is a critical target of pathogen-responsive MAPK cascade in plant basal defense. PLoS Pathog. *10*, e1004243.

Wang, H.-J., Hsu, Y.W., Guo, C.L., Jane, W.N., Wang, H., Jiang, L., and Jauh, G.Y. (2017). VPS36-dependent multivesicular bodies are critical for plasma-membrane protein turnover and vacuolar biogenesis. Plant Physiol. *173*, 566–581.

Wiermer, M., Feys, B.J., and Parker, J.E. (2005). Plant immunity: the EDS1 regulatory node. Curr. Opin. Plant Biol. *8*, 383–389.

Zeier, J. (2013). New insights into the regulation of plant immunity by amino acid metabolic pathways. Plant Cell Environ. *36*, 2085–2103.

Zhang, Z., Feechan, A., Pedersen, C., Newman, M.-A., Qiu, J.L., Olesen, K.L., and Thordal-Christensen, H. (2007). A SNARE-protein has opposing functions in penetration resistance and defence signalling pathways. Plant J. *49*, 302–312.

Zhang, Z., Lenk, A., Andersson, M.X., Gjetting, T., Pedersen, C., Nielsen, M.E., Newman, M.-A., Hou, B.-H., Somerville, S.C., and Thordal-Christensen, H. (2008). A lesion-mimic syntaxin double mutant in *Arabidopsis* reveals novel complexity of pathogen defense signaling. Mol. Plant *1*, 510–527.

Zhang, Z., Wu, Y., Gao, M., Zhang, J., Kong, Q., Liu, Y., Ba, H., Zhou, J., and Zhang, Y. (2012). Disruption of PAMP-induced MAP kinase cascade by a *Pseudomonas syringae* effector activates plant immunity mediated by the NB-LRR protein SUMM2. Cell Host Microbe *11*, 253–263.

Zhu, X., Yin, J., Liang, S., Liang, R., Zhou, X., Chen, Z., Zhao, W., Wang, J., Li, W., He, M., et al. (2016). The multivesicular bodies (MVBs)-localized AAA ATPase LRD6-6 inhibits immunity and cell death likely through regulating MVBs-mediated vesicular trafficking in rice. PLoS Genet. *12*, e1006311.

STAR★METHODS

KEY RESOURCES TABLE

REAGENT or RESOURCE	SOURCE	IDENTIFIER
Antibodies		
Anti-AMSH3 Rabbit polyclonal	Isono et al. (2010)	N/A
Anti-ubiquitin Rabbit polyclonal	Sigma-Aldrich	Cat# Sigma-U5379
Anti-GFP Mouse monoclonal	Santa Cruz Biotechnology	Cat# sc-9996
Anti-RIN4 Goat polyclonal	Santa Cruz Biotechnology	Cat# sc-27369
Anti-PEN1 Rabbit polyclonal	Zhang et al. (2007)	N/A
Anti-HA Rat monoclonal	Chromotek	Cat# 7C9
Anti-GST Mouse monoclonal	Genscript	Cat# A00865-40
Anti-Gal4-BD (GBD) Mouse monoclonal	Clontech	Cat# 630403
Anti-Rat AP-conjugated	Sigma-Aldrich	Cat# A3687
Anti-Rabbit HRP-conjugated	Santa Cruz Biotechnology	Cat# sc-2004
Anti-Mouse HRP-conjugated	Sigma-Aldrich	Cat# A4416
Anti-Goat AP-conjugated	Santa Cruz Biotechnology	Cat# sc-2771
Bacterial and Virus Strains		
Pst DC3000 AvrRpm1	Grant et al. (1995)	N/A
Pst DC3000 AvrRpt2	Kunkel et al. (1993)	N/A
Pst DC3000 AvrRps4	Hinsch and Staskawicz (1996)	N/A
Pst DC3000 AvrRphB	Simonich and Innes (1995)	N/A
Agrobacterium tumefaciens GV3101 pMP90	Koncz and Schell (1986)	N/A
One Shot TOP10	Invitrogen	Cat# K2400-20
Escherichia coli Rosetta 2	Merck	Cat# 71405
Chemicals, Peptides, and Recombinant Proteins		
Gateway BP Clonase II Enzyme Mix	ThermoFisher Scientific	Cat# 11789100
Gateway LR Clonase II Enzyme Mix	ThermoFisher Scientific	Cat# 11791100
Beta-estradiol	Sigma-Aldrich	Cat# E8875
Trypan blue	Sigma-Aldrich	Cat# T-0776
c0mplete protease inhibitor cocktail	Sigma-Aldrich	Cat# 11697498001
Protino Glutathione Agarose 4B	Machery-Nagel	Cat# 745500.10
K48-ubiquitin tetramer	Boston Biochem	Cat# UC-210B
K63-ubiquitin trimer	Boston Biochem	Cat# UC-315B
TAMRA-labeled K63-ubiquitin dimer	R&D Systems	Cat# P62988
IPTG	Sigma-Aldrich	Cat# I6758
BASTA	Bayer	Cat# L4872
BTH	Syngenta	Cat# A9180A
Critical Commercial Assays		
QuikChange II XL Site-Directed Mutagenesis kit	Agilent	Cat# 200521
SMART MMLV RT kit	Clontech	Cat# 634901
5x HOT FIREPol EvaGreen qPCR Mix Plus	Solis BioDyne	Cat# 08-24-00001
Experimental Models: Organisms/Strains		
Arabidopsis thaliana Col-0 wild-type	N/A	N/A
A. thaliana Col-0 *amsh3-3*	This study	N/A
A. thaliana Col-0 *amsh3-4*	This study	N/A
A. thaliana Col-0 *amsh3-1*	Isono et al. (2010)	N/A
A. thaliana Col-0 *ndr1-1*	Century et al. (1997)	N/A

(*Continued on next page*)

Continued

REAGENT or RESOURCE	SOURCE	IDENTIFIER
A. thaliana Col-0 *eds1-2*	Bartsch et al. (2006)	N/A
A. thaliana Col-0 *acd11-2*	Brodersen et al. (2005)	N/A
A. thaliana Col-0 *lsd1-2*	Torres et al. (2005)	N/A
A. thaliana Col-0 *pen1-1 syp122-1*	Zhang et al. (2007)	N/A
A. thaliana Ler *pen1-1 syp122-1*	Zhang et al. (2007)	N/A
A. thaliana Col-0 *pen1-1 syp122-1* 35S::*AMSH3*	This study	N/A
A. thaliana Col-0 *pen1-1 syp122-1 eds1-2*	Zhang et al. (2007)	N/A
A. thaliana Col-0 *pen1-1 syp122-1 fmo1-1*	Zhang et al. (2008)	N/A
A. thaliana Col-0 *pen1-1 syp122-1 npr1-1*	Zhang et al. (2007)	N/A
A. thaliana Col-0 *pen1-1 syp122-1 pad4-19*	Zhang et al. (2008)	N/A
A. thaliana Col-0 *pen1-1 syp122-1 sid2-1*	Zhang et al. (2007)	N/A
A. thaliana Col-0 *pen1-1 syp122-1 amsh3-3*	This study	N/A
A. thaliana Col-0 *pen1-1 syp122-1 amsh3-4*	This study	N/A
A. thaliana Col-0 *pen1-1 syp122-1 eds1-2 amsh3-3*	This study	N/A
A. thaliana Col-0 *pen1-1 syp122-1 fmo1-1 amsh3-3*	This study	N/A
A. thaliana Col-0 *pen1-1 syp122-1 npr1-1 amsh3-3*	This study	N/A
A. thaliana Col-0 *pen1-1 syp122-1 pad4-19 amsh3-3*	This study	N/A
A. thaliana Col-0 *pen1-1 syp122-1 sid2-1 amsh3-3*	This study	N/A
A. thaliana Col-0 *amsh3-1 eds1-2*	This study	N/A
Oligonucleotides		
Primers used in this study, see Table S1	This study	N/A
Recombinant DNA		
pENTR-D-TOPO	ThermoFisher Scientific	Cat# K2400-20
pK7WGF2	Karimi et al. (2007)	N/A
pB2GW7: 35S-AMSH3	This study	N/A
pK7WGR2: p35S-RFP	Karimi et al. (2007)	N/A
pK7WGR2: p35S-RFP-AMSH3 (WT)	This study	N/A
pK7WGR2: p35S-RFP-AMSH3 (P214S)	This study	N/A
pK7WGR2: p35S-RFP-AMSH3 (P445S)	This study	N/A
pK7WGF2: p35S-GFP	This study	N/A
pK7WGF2: p35S-GFP-SKD1 (E232Q)	This study	N/A
pEst-T7-RPM1-YFP-HA	Gao et al. (2011)	N/A
pEst-T7-RPM1 (D505V)-YFP-HA	Gao et al. (2011)	N/A
pDEST-ACT2	Robertson (2004)	N/A
pDEST-ACT2: HA-GAD-AMSH3 (WT)	This study	N/A
pDEST-ACT2: HA-GAD-AMSH3 (P214S)	This study	N/A
pDEST-ACT2: HA-GAD-AMSH3 (P445S)	This study	N/A
pGBKT7: GBD	Kalinowska et al. (2015)	N/A
pGBKT7: GBD-ALIX	Kalinowska et al. (2015)	N/A
pGBKT7: GBD-VPS2.1	Katsiarimpa et al. (2013)	N/A
pT7-GST-AMSH3	This study	N/A
pT7-GST-AMSH4 (P214S)	This study	N/A
pT7-GST-AMSH3 (P445S)	This study	N/A
Software and Algorithms		
R	The R Project for Statistical Computing	Ver. 3.4.3

CONTACT FOR REAGENT AND RESOURCE SHARING

Further information and requests for resources and reagents should be directed to and will be fulfilled by the Lead Contact, Hans Thordal-Christensen (htc@plen.ku.dk).

EXPERIMENTAL MODEL AND SUBJECT DETAILS

Arabidopsis

All *A. thaliana* (L.) Heynh. mutants and transgenic lines listed above were sown in soil, then incubated at 4°C for 3 days, and subsequently grown in growth chamber at 21°C and 70% relative humidity under short-day conditions with 8-hr light at 125 μEinstein $s^{-1}m^{-2}$.

Nicotiana benthamiana

N. benthamiana plants were greenhouse-grown in soil under long-day conditions (16-hr light) at 24°C.

Bacterial strains

Pseudomonas syringae pv. *tomato* (*Pst*) DC3000 expressing either AvrRpm1, AvrRpt2, AvrRps4, or AvrPphB were grown on LB plates with 100 μg/ml rifampicin and 50 μg/ml kanamycin for 2 days for inoculation.

METHOD DETAILS

Map-based cloning

To identify the *ssd4-1* mutation that suppressed the *pen1 syp122* phenotype, an F_2 population from a cross between *pen1 syp122 ssd4-1* in ecotype Columbia (Col-0) and *pen1-1 syp122-1* backcrossed into ecotype Landsberg *erecta* (Ler) (Zhang et al., 2008) was used. Initial mapping positioned *SSD4* on chromosome 4 in an interval between the markers, ciw6 (At4g13570) and FCA8 (At4g17200). Subsequent fine-mapping placed *SSD4* in a region of 17 genes spanning from At4g16130 to At4g16215. The *ssd4-1* mutation was identified after PCR-amplification and sequencing of all coding sequences in the interval based on genomic DNA.

BTH-treatment

Plants were sprayed with 300 μM BTH or water until the leaves were fully wet. The rosette fresh weight was determined after cutting the rosette from the stem.

Plasmid constructs

All cloning was done using the Gateway system (Thermo Fisher Scientific). The coding sequence for AMSH3 was cloned from cDNA into pENTR-D-TOPO, and those for AMSH3-3 and AMSH3-4 were generated by site-directed mutagenesis using the QuikChange II Clonase kit. All were transferred to pDEST15 (GST-tag), using the LR-II kit (Invitrogen), and transformed into the *E. coli* Rosetta 2 strain (Merck) for protein expression. Coding sequences for N-terminally GFP-tagged $SKD1^{E232Q}$ (Katsiarimpa et al., 2011) and the AMSH3 versions were generated by recombining the pENTR clones with pK7WGF2 and pK7WGR2, respectively, using the LR-II Clonase kit. These constructs were then transformed into *Agrobacterium tumefaciens* GV3101 pMP90. For yeast two-hybrid assays, the AMSH3 alleles were introduced into the pDEST-ACT2 plasmid (Robertson, 2004) using the LR-II Clonase kit. Primers were synthesized at TAG Copenhagen (TAGC.dk).

Stable transformation of *A. thaliana* and transient protein expression in *N. benthamiana*

The *A. tumefaciens* strain GV3101 harboring binary protein expression vectors was grown overnight on LB plates (10 g tryptone, 5 g yeast extract, 5 g NaCl, 15 g Agar per liter) containing 100 μg/ml rifampicin, 100 μg/ml spectinomycin, and 25 μg/ml gentamycin. The cells were harvested and resuspended in 10 mM $MgCl_2$. Stable transformants of *A. thaliana* were obtained after floral dipping and subsequent selection of plants germinating from the harvested seeds on MS plates containing Basta (60 μg/ml) (Clough and Bent, 1998). Co-expression in *N. benthamiana* was obtained by mixing the *A. tumefaciens* strains (each with an OD_{600} = 0.3) with the indicated plasmids, which then were infiltrated with a needleless syringe into leaves of 4-5-week-old plants.

Bacterial growth assays

Pst DC3000 expressing either AvrRpm1, AvrRpt2, AvrRps4, or AvrPphB were harvested and resuspended in 10 mM $MgCl_2$ and 0.01% v/v Silwet L-77 to 10^8 CFU/ml and spray-inoculated onto plants. To maintain high humidity the plants were covered with a translucent lid for one day. Bacterial populations within the leaves were determined 3 dpi. For each repeat, four leaf discs size 3 were sampled from the same rosette and ground in 200 μl 10 mM $MgCl_2$, using a pistle mounted on an electric drill, while adding 800 μl of 10 mM $MgCl_2$. A 6-times serial dilution was performed. Twenty microliters of each of the six dilutions were plated on LB plates supplemented with appropriate antibiotics. The colonies were counted 2-3 days after plating.

Ion leakage experiments

A. thaliana plants were infiltrated with 10^8 CFU/ml bacteria and five leaf discs harvested for each repeat using a cork-borer size 4. The discs were floated on water for 60 min. and then transferred to a 12 mL culture tube containing 5 mL water (5 discs per tube = one repeat). Experiments in *N. benthamiana* were performed in the same way 2 dpi with *A. tumefaciens* harboring the indicated plasmids. The expression of RPM1 or RPM1^{D505V} was induced with 40 μM β-Estradiol 2 hours prior to the leaf discs being cored and floated as described above. The change in conductivity of the solution was measured with a conductivity meter (CRM210, Radiometer) at the indicated time points.

Yeast two-hybrid assay

The interaction between AMSH3 versions and other ESCRT components were analyzed by co-transforming *Saccharomyces cerevisiae* Y190 with pDEST-ACT2:AMSH3, pDEST-ACT2:AMHS3-3 or pDEST-ACT2:AMSH3-4 combined with pGBKT7:VSP2.1 (Katsiarimpa et al., 2013) or pGBKT7:Alix (Kalinowska et al., 2015). The yeast two-hybrid assay was performed on synthetic complete medium without leucine and tryptophan (-LW) as well as histidine (-LWH). Higher stringency condition was obtained by adding 3-amino-1,2,4-triazole (3AT).

Total protein extraction

Total protein from *N. benthamiana* was extracted by grinding three leaf discs, made using cork-borer size 3, in liquid nitrogen with metal beads in 1.5 mL Eppendorf tubes using a Retsch mill. Two hundred and fifty microliters of 2 x modified Laemmli buffer (0.24 M Tris-Cl, pH 6.8, 6% SDS, 30% glycerol, 16% β-mercaptoethanol, 0.006% bromophenol blue, 10 M urea) were added to the samples, which then were heated for 5 min. at 95°C. The samples were then subjected to SDS-PAGE and western blot analysis as described below.

Total protein was extracted from *A. thaliana* by grinding 4-5-week-old plant leaf tissue in liquid nitrogen using a mortar and pestle. The proteins were extracted by incubation in cold buffer (100 mM Tris-HCl pH 7.5, 150 mM NaCl, 5 mM EDTA, 5% glycerol, 0.5% Triton X-100, 10 mM DTT and 1x c0mplete protease inhibitor cocktail (Roche)) for 30 min. at 4°C. The protein concentration of supernatants from a 12,000 x g centrifugation, for 20 min. at 4°C, was determined using BioRad's Bradford reagent.

For western blots, samples were heated for 5 min. at 95°C with 4x RunBlue LDS sample buffer (40% Glycerol, 4% LDS, 0.8 M Triethanolamine-Cl pH 7.6, 4% Ficoll-400, 0.025% Phenol Red, 0.025% Coomassie Brilliant Blue G250, 2 mM EDTA-2Na). The proteins were separated on Any kD Mini-PROTEAN® TGX Precast Protein Gels (BioRad) or 10% SDS-PAGE gels (Expedeon) and subsequently transferred to PVDF membranes (BioRad) using Trans-Blot Turbo Transfer System (BioRad). Immuno-blots were performed using 1:1000 anti-PEN1 (Zhang et al., 2007), 1:5000 anti-GFP (Santa Cruz Biotech.), 1:1000 anti-ubiquitin (Sigma-Aldrich), 1:1500 anti-AMSH3 (Isono et al., 2010), 1:1000 anti-HA (Chromotek), 1:1000 anti-RIN4 (Santa Cruz Biotech.), 1:1000 anti-Gal4 BD (GBD) (Santa Cruz Biotech.), 1:1000 anti-HA-HRP (Roche) and 1:2000 anti-YFP (Agrisera). Blots were reacted with AP- or HRP-conjugated secondary antibodies and revealed with BCIP/NBT (Promega) or Clarity Western ECL (Biorad), respectively.

RNA isolation and quantitative PCR

Total RNA was isolated from *A. thaliana* tissue using TRIzol (Ambion) and RQ1 RNase-free DNase (Promega)-treated. cDNA was synthesized using the SMART™ MMLV RT kit (Clontech) and an oligo(dT) primer.

Transcript quantification was performed using the 5x HOT FIREPol EvaGreen qPCR Mix Plus (SOLIS BIODYNE) on a Stratagene MX3000P real-time PCR detection system. Gene specific primers are described in Table S1. We used the At4g26410 transcript as internal control (Czechowski et al., 2005).

DUB assays

Over-night cultures (OD_{600} = 0.6) of *E. coli* Rosetta 2 expressing the three versions of AMSH3 were supplied with IPTG to 500 μM and incubated at 18°C for another 18 h. The cells were harvested and resuspended in Buffer A (50 mM Tris-HCl, 100 mM NaCl, 10% glycerol) supplied to 1x c0mplete protease inhibitor cocktail (Roche) and 0.5% Triton X-100. Cells were sonicated for 10 × 15 s. at setting 5 of 10, and the cellular debris pelleted at 12.500 x g for 10 min. Hundred microliters Protino® Glutathione Agarose 4B (Macherey-Nagel) were added to the supernatant, and the slurry was incubated by rolling for 2 h. at 4°C. The beads were pelleted by a 500 x g centrifugation for 5 min. and washed three times in Buffer A. The bound proteins were eluted in 200 mM glutathione, pH 8.0. Gels with the purified proteins are shown in Figures 4B and 4C and S5.

Deubiquitination experiments were performed using K48- or K63-linked ubiquitin tetramer and trimer chains, respectively (Boston Biochem.). Two hundred fifty nanogram of ubiquitin chains were mixed with 2 pmol of *E. coli*-expressed AMSH proteins and incubated for the indicated time in a DUB Assay Buffer (50 mMTris-HCl pH 7.2, 25 mM KCl, 5 mM $MgCl_2$, 1 mM DTT) at 30°C. The reaction mixture was subjected to immunoblotting using an anti-Ubiquitin antibody. In a second deubiquitination assay 400 nM of K63-linked di-ubiquitin FRET TAMRA (position 3) (Boston Biochem) was mixed with 50 nM of *E. coli*-expressed AMSH proteins in a TAMRA DUB Buffer (50 mM Tris-HCl pH 7.5, 100 mM NaCl, 0.1% Pluronic F-127, 1 mM Tris (2-carboxyethyl) phosphine (TCEP)) and the fluorescence intensity was measured every minute for 120 minutes.

Protein localization in *N. benthamiana*

RFP:AMSH3 wild-type and mutant versions were co-localized with GFP:SKD1^{E232Q} in leaves of 4-5-week-old *N. benthamiana*, infiltrated with *A. tumefaciens* harboring the desired constructs. Two days later, leaf discs were punched using cork-borer size 4, and after water mounting, imaged on the abaxial side with an inverted Leica SP-5 confocal laser-scanning microscope. GFP was excited with the 488 nm argon-laser and fluorescence emission collected between 500 and 550 nm. RFP was excited at 543 nm and fluorescence emission collected between 640 and 645 nm. To visualize GFP and RFP simultaneously, Sequential Scan Mode was used. The confocal images were edited in Leica AF Lite (Version 2.6.3 build 8173) and Adobe Photoshop CS5.1 (64 Bit).

Structural homology modeling

The AMSH3 protein sequence was submitted to the online server SWISS-MODEL (Biasini et al., 2014). The best model with a QMEAN score of −2.00 and 51.83% identity was based on the crystal structure of *Schizosaccharomyces pombe* AMSH-like protease sst2 (4nql.1.A). The model encompassing AMSH3$^{318-507}$ was visualized in Swiss-PDBViewer V4.1.0 (https://www.expasy.org/spdv/).

QUANTIFICATION AND STATISTICAL ANALYSIS

The numbers of biological repeats (n) are provided in each figure legend. For transcript analyses, each biological repeat is based on an RNA sample extracted from four plants. For plant weight, repeats are individual plants. For bacterial growth, each repeat is based on four leaf discs from one plant. For ion leakage, each repeat is based on five leaf discs. Data are presented as means ± standard error (SE). We performed one-way analysis of variance (ANOVA) with a Tukey HSD post hoc test using R (http://www.R-project.org/). We employed an alpha of 0.05 as cut-off for significance.